Article

Not peer-reviewed version

Assessment of the Environmental Impacts of the Launch of the “Soyuz-2.1a” Launch Vehicle with the “Progress MS-29” Cargo Spacecraft in Kazakhstan

Aliya Kalizhanova , Murat Kunelbayev , Anar Utegenova , Ainur Kozbakova * , Serik Daruish

Posted Date: 14 April 2026

doi: 10.20944/preprints202604.1023.v1

Keywords: Baikonur; petroleum products; nitrogen dioxide; before-after control impact; regression on order statistics; geographic information system; hazard quotient risk

 doi:10.20944/preprints202604.1023.v1

Article

Assessment of the Environmental Impacts of the Launch of the "Soyuz-2.1a" Launch Vehicle with the "Progress MS-29" Cargo Spacecraft in Kazakhstan

Aliya Kalizhanova [1], Murat Kunelbayev [2], Anar Utegenova [3], Ainur Kozbakova [4,*] and Serik Daruish [5]

[1] Institute of Information and Computational Technologies CS MSHE RK, Almaty University of Energy and Communications named after G. Daukeyev, Almaty, Kazakhstan
[2] Institute of Information and Computational Technologies CS MSHE RK, Almaty, Kazakhstan
[3] Institute of Information and Computational Technologies CS MSHE RK, Almaty Technological University, Almaty, Kazakhstan
[4] Institute of Information and Computational Technologies CS MSHE RK, Satbayev University, Almaty, Kazakhstan
[5] Institute of Information and Computational Technologies CS MSHE RK, Al Farabi Kazakh National University, Almaty, Kazakhstan
* Correspondence: ajnurkozbakova@gmail.com; Tel.: +7-7788889298

Abstract

The relevance of this study stems from the need for a scientifically sound assessment of the environmental risks associated with launch vehicle launches and for ensuring the environmental safety of areas potentially impacted by space activities. Comprehensive environmental monitoring in the impact areas of rocket parts and adjacent populated areas is particularly important, taking into account natural and climatic factors and the spatial heterogeneity of pollution. This study assessed the environmental impacts of the "Soyuz-2.1a" launch with the ""Progress MS-29"" cargo spacecraft in Kazakhstan based on integrated field research and geoinformation analysis. The study covered the launch area, adjacent populated areas, and the impact zone. A before-after control impact (BACI) design with distance stratification and wind pattern considerations was used to identify post-launch changes. Data containing values below the detection and quantification limits were processed using censored observation analysis methods (ROS Regression on Order Statistics and Kaplan-Meier). A spatial analysis of pollutant distribution was conducted, with thermal field and contour maps generated, revealing the anisotropy of the risk field and localized areas of increased environmental stress. An integrated environmental risk (HQ) metric was used to compare the state of atmospheric air, water, and soil, providing a unified approach to interpreting the results. It was established that the post-launch impact is localized and time-limited, with the greatest sensitivity observed in the soil component in the first period after launch. Measures are recommended to temporarily restrict access to areas of increased stress, conduct primary reclamation, and organize staged environmental monitoring using WebGIS technologies to support management decisions. The scientific novelty of the work lies in the development of an anisotropic model for assessing environmental risk taking into account wind rose and in the integration of methods for analyzing censored data into a unified system for monitoring environmental components.

Keywords: Baikonur; petroleum products; nitrogen dioxide; before-after control impact; regression on order statistics; geographic information system; hazard quotient risk

 doi:10.20944/preprints202604.1023.v1

1. Introduction

The impact of rocket and space activities on the environment in Kazakhstan remains a pressing scientific and applied issue. Regular launches from the Baikonur Cosmodrome are accompanied by atmospheric emissions, mechanical destruction of the soil cover, and potential contamination by rocket fuel components. The objective of this study is to conduct a comprehensive assessment of the environmental situation during the launch of the “Soyuz-2.1a” launch vehicle with the ““Progress MS-29”” spacecraft. Article [1] presents the results of the “Soyuz-FG” launch vehicle and “Soyuz MS-10” spacecraft accident in the Ulytau region of Kazakhstan, identifying two local fuel spill zones. No significant differences in the exchange forms of Ca and Mg or in cation exchange capacity were found between the seasonal samples. The obtained results are informative for the development of remediation programs for arid landscapes and for planning monitoring in areas of regular stage landings and emergency impacts. In [2], a method for determining rocket kerosene (RG-1 and T-1) in soil was developed using static headspace sampling followed by gas chromatography–mass spectrometry (GC–MS). It was shown that analysis of the vapor phase above a solid sample is preferable to ultrasonic extraction with methanol and analysis of the equilibrium vapor phase above the extract. In [3], the identification of semi-volatile fuels in soil based on the distribution of sesquiterpanane biomarkers was demonstrated. Extraction with dichloromethane and GC–MS revealed markers in RG-1, T-1, TS-1 and diesel. The biomarker profiles are specific and are preserved during soil transformation; profile parameters were proposed for reliable identification at any stage. Article [4] presents an overview of the environmental impacts of space launches, focusing on emissions from solid and liquid rocket propellants. It is shown that stratospheric ozone depletion is the best-studied and most acute effect: the contribution of liquid rocket engines has been confirmed, but solid engines cause losses orders of magnitude higher. Environmental tradeoffs in the selection of launch systems are discussed, and gaps in knowledge (climate, ecotoxicity, health risks) are identified. Article [5] examines the environmental impacts of launch vehicle accidents during the boost phase of flight (debris fall, fuel spills, emissions), and presents an approach to damage assessment and measures for its mitigation/elimination. A set of routine indicators of the "hydrocarbon status" of soils (bitumoids, polycyclic aromatic hydrocarbons PAHs, gaseous hydrocarbons) is proposed, tested at eight sites ranging from forest to dry steppe. The hydrocarbon status (HCS), as an integral indicator, reflects climatic and geomorphological conditions, soil properties, and anthropogenic load [6]. The work [7] proposed a set of routinely measured indicators of the "hydrocarbon status" of soils (bitumoids, PAHs, and gas hydrocarbons), which are used to assess natural and anthropogenic impacts. Studies at eight sites from forest to dry steppe showed that HCS, like humus/salt status, serves as an integral characteristic of soils, reflecting climatic and geomorphological conditions, soil properties, and pollution levels. The article [8] examines the rocket and technical context of Nitrosodimethylamine (NDMA) its use in hypergolic vapors (UDMH - Unsymmetrical Dimethylhydrazine /N_2O_4), pathways of entry into the environment (flare emissions, spills during stage falls and accidents, discharge of residues), and subsequent transformation to nitrosamines. Article [9] discusses “heptyl” (NDMA, UDMH) as a widely used rocket propellant, which is prone to irreversible wetting with loss of properties, which limits its long-term storage. Article [10] assessed potentially mineralizable carbon (PMC) and nitrogen (PMN) in Eurasian steppe soils across 41 samples (Ukraine, Kazakhstan; cropland, forest, meadow, desert) after 133-day incubation with CO_2 and mineral N monitoring. Article [11] found that exposure of watercress and zucchini to UDMH rapidly and at all concentrations results in the formation of 1-methyl-1H-1,2,4-triazole, a reliable marker of UDMH contamination (according to GC-MS data). In [12], the leasing regime and Roscosmos's control create a closed environmental policy around Baikonur, where Proton accidents and the risk of UDMH coexist with the suppression of criticism and the absence of independent science. In [13], the concept of Baikonur's "internal offshore" is substantiated: lease deals between Russia and Kazakhstan convert the Soviet legacy into a closed governance regime, where the vast lands of the "drop zones" serve global flows of launches, capital, and waste. In [14], it is

 doi:10.20944/preprints202604.1023.v1

shown that behind the façade of rocket heroics lies the land and infrastructure of launches. Since the 1950s, "drop zones" in the Kazakh steppe have received stages and toxic fuel residues from launches from Baikonur. It is argued that post-Soviet lease agreements between Russia and Kazakhstan have transformed this Soviet facility into an "intracontinental offshore"—a privatized space with offshore privileges and elements of de facto extraterritoriality. The study [15] analyzes the environmental safety of soils exposed to UDMH (heptyl): domestic methods for determining its mass fraction are compared, the behavior of the substance and its transformation pathways in ecosystems are considered, and practical experience in remediation is systematized. The risk of secondary UDMH formation during the sample preparation stage is separately noted, and it is shown that the duration of contamination persistence is determined by the soil type: in acidic peatlands it persists longer, while in alkaline peatlands it persists much less. The work [16] provides a concise assessment of the environmental aspects of kerosene use in the aerospace sector. It is shown that the key risks are caused by emissions and leaks in aviation, as well as spills at the impact sites of the first stages of launch vehicles (while the second and third stages usually do not affect terrestrial ecosystems). The article [17] shows that oxidative methods for UDMH purification were assessed based on residual fuel, ignoring many nitrogen-containing transformation products. The article [18] shows that in coastal salt marshes of the Bohai coast, soils under vegetation, compared to "bare" soils, have lower EC - Electrical Conductivity /salt/SAR - Sodium Adsorption Ratio/density and higher pH, organic matter, MWD -Mean Weight Diameter and Ks -Saturated hydraulic conductivity. RDA (Redundancy Analysis)/ SEM (Structural Equation Modeling) analyses revealed two opposing sets of features and confirmed that the key determinants of salinity are organic matter and density, with their combined effect being stronger than their individual effects, which is important for desalinization strategies. The article [19] examines how "space industrialization" affects the Earth's environment. The article discusses the growth of space debris, light pollution of the night sky, the possible impact of launches and debris burnup on the atmosphere and ozone layer, radiation risks from nuclear sources on spacecraft and the effects of expanding space tourism. The authors call for measures to reduce these impacts and stricter regulation. The article [20] shows that spectrofluorimetric in combination with multivariate data analysis can quickly predict the oxidative stability of oils and biodiesel. The article [21] systematizes the oxidation pathways of UDMH and its (often highly toxic) products despite the disparity of data, some of which is only hypothetical. Detection environments, confirmed schemes and toxicity are summarized; it is emphasized that prediction without experiment is unreliable, and understanding the transformations is necessary for risk identification and mitigation. Article [22] notes that hydrazine and its derivatives—monomethylhydrazine (MMH) and unsymmetrical dimethylhydrazine (UDMH)—are highly toxic and are widely used as rocket fuels in military and aerospace technology. Article [23] examines laboratory methods for assessing the hydrocarbon status of soils—the total content and composition of bitumoids, individual hydrocarbons, and gases. The most applicable approaches are described: luminescence-bituminological analysis and low-temperature spectrofluorimetric.

2. Materials and Methods

Three main areas were selected for the study of launch vehicle impact zones: the cosmodrome launch site, the first stage impact area, and populated areas located near the flight trajectory. This choice was driven by the need for a comprehensive analysis—from local processing sites to populated areas. In the launch site (site 31), the impact of fueling and launch operations on air and soil conditions was studied. In the first stage impact area (zone U-25, Ulytau), fuel component spills, mechanical damage to the soil, and localized fires were assessed. In the populated areas of Baikonur, Toretam, Akai, Zhezkazgan, and Talap, air, water, and soil quality were measured to determine the potential impact of the launch on living conditions.

To obtain reliable data, sampling was carried out according to standardized methods and state standards. Soil samples were collected from the upper soil layer (0–20 cm), corresponding to the zone

 doi:10.20944/preprints202604.1023.v1

of greatest pollutant accumulation, using State Standards SS(GOST) 17.4.3.01-2017 and SS(GOST) 17.4.4.02-2017. In populated areas, pooled samples were collected from four locations, allowing for spatial variability in pollution to be accounted for. Drinking water samples were collected in accordance with Standard of the Republic of Kazakhstan SS(GOST) R 51592-2003 from centralized networks and individual sources, using sterile containers and observing preservation conditions. To monitor air quality, measurements were taken at a height of 1.5 m above the ground, corresponding to the human breathing zone, and were conducted in three time periods: before launch, immediately after, and 24 hours later. A wide range of measuring instruments was used for analysis, providing both rapid assessments and detailed laboratory studies. The Automatic Continuous Monitoring Gas Analyzer Model-4 (ACMGA-4) gas analyzer was used to record concentrations of nitrogen oxides and hydrocarbons in the ground layer of the atmosphere. The Electronic meteorometer stationary MES-200A meteorological meter recorded meteorological parameters (temperature, humidity, wind speed and direction) necessary for the accurate interpretation of pollutant propagation. Indicator tubes compliant with SS(GOST) 12.1.014-84 provided rapid monitoring of harmful substance levels in the air. For more complex analyses, a “Color Yauza” ion liquid chromatograph with amperometric and spectrophotometric detectors was used, enabling the determination of 1,1-dimethylhydrazine and its derivatives. Nitrosodimethylamine concentrations were determined with a Spekolo-1500 spectrophotometer, and petroleum products with a “Fluorat-02-3M” fluorimeter. In addition, PU-4E and AM-5 aspirators were used to collect air samples in sealed containers.

A combination of physicochemical methods was used to assess environmental conditions. Ion chromatography was used to determine hydrazines and their derivatives in air and soil. Spectrophotometric methods allowed for the detection of nitrogen-containing compounds, including carcinogenic nitroso compounds. Fluorimetric analysis provided highly sensitive detection of petroleum products in water and soil. Electrometric methods were also used to measure the pH and conductivity of aqueous soil extracts, as well as complexometry to determine metal ion content. All methods were calibrated using standard samples and precision controlled using replicate measurements. A Garmin GPSmap 60CSx satellite receiver was used to record the coordinates of the collected samples, ensuring precise georeferencing of the data. This allowed for the creation of a digital map of the surveyed areas and the comparison of the spatial distribution of pollutants. All measurements were performed in triplicate. The results are presented as mean values with standard deviations. To assess the environmental significance, maximum permissible concentrations (MPC) for air, soil and water were used, as well as Approximate safe exposure level (ASEL) for atmospheric air in populated areas.

Figure 1 illustrates the environmental monitoring methodology sequence. First, the survey zones are defined—the site area, the step fall area, and populated areas. Then, soil, water, and air samples are collected, transported, and stored. In the laboratory, the samples are analyzed using ion chromatography, spectrophotometry, and fluorimetry. The obtained results are statistically processed and compared with the MPC and ASEL. The final stage includes an environmental impact assessment and verification of compliance with sanitary standards.

 doi:10.20944/preprints202604.1023.v1

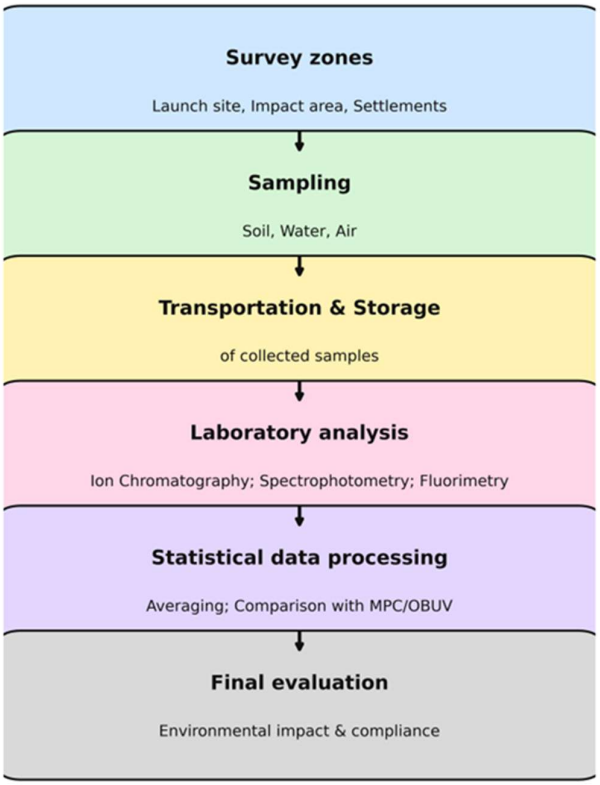

Figure 1. Environmental Monitoring Methodology Sequence.

Figure 2 shows the environmental monitoring architecture. At the field level, a ACMGA-4 gas analyzer, an MES-200A meteorometer, indicator tubes, and soil and water samplers are used. At the laboratory level, samples are analyzed using a chromatograph, spectrophotometer, and fluorimeter. The information level includes statistical data processing, comparison of results with MPC and ASEL standards, and the generation of a final report.

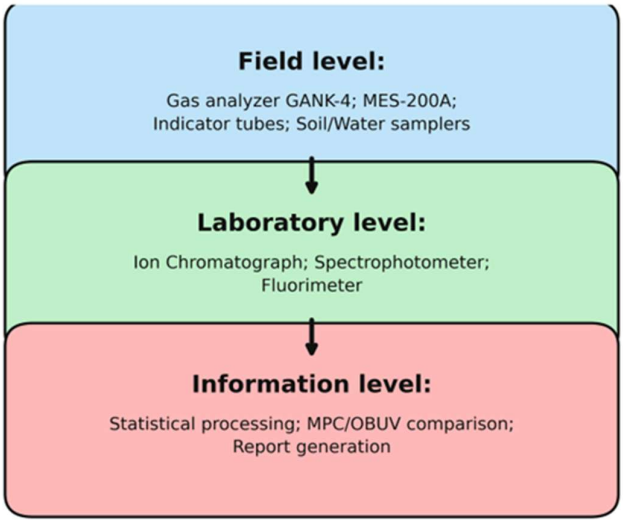

Figure 2. Environmental Monitoring Architecture.

Figure 3 describes the full cycle of environmental support for launch. The preparatory stage includes planning, selection of observation points, and review of the regulatory framework. Next,

 doi:10.20944/preprints202604.1023.v1

samples are collected in impact zones and field measurements are taken using instruments. In the next stage, the samples are analyzed in the laboratory using chromatography, spectrophotometry, and fluorimetry. The results are statistically processed and compared with MPC and ASEL standards. The final step involves drawing conclusions and developing recommendations to minimize the impact.

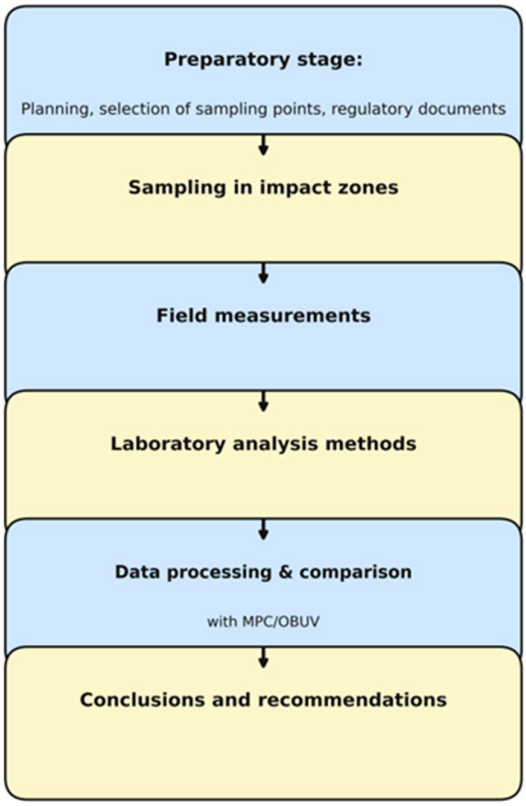

Figure 3. Full Cycle of Environmental Support for Launch.

Figure 4 shows the general process of environmental monitoring during a rocket launch. At the input are sources of pollution—spills of rocket fuel components (e.g., UDMH) and combustion products. These impact the natural environments: soil, air, and water, where changes in parameters are recorded. At the output, monitoring results are compiled in the form of tables, graphs, and maps, which allow for an assessment of the impact level and the development of risk mitigation recommendations.

Figure 4. General process of environmental monitoring during a rocket launch.

2.1. Inversion Estimate of Emission Intensity Q Based on Field Data*

This subsection describes the inversion formulation of the problem: the emission intensity of source Q (g/s) is determined from field observations, after which the reconstructed concentration and risk fields are calculated, linked to the assessed source.

 doi:10.20944/preprints202604.1023.v1

2.1.1. Data for Inversion

For each monitoring point i, an increment relative to the background is generated using the BACI (T-/T+) scheme:

$$\Delta C_i = C_i(T+) - C_i(T-) \quad (1)$$

Here, $C_i(T+)$ is the concentration (or contamination indicator) after the event, and $C_i(T-)$ is the background value before the event. For values below the detection limit (<LOD limit of detection) or below the limit of quantification (<LOQ limit of quantification), it is recommended to use unbiased estimates (e.g., Regression on order statistics (ROS) or Kaplan-Meier) to avoid underestimating ΔC_i.

2.2.2. Single-Emission Response Model

Since in dispersion models, the ground-level concentration is linear with respect to the source intensity Q, a response to a single emission gi is introduced:

$$C_i^{model}(Q) = Q \cdot g_i, \quad g_i = C_i^{model}(Q = 1) \quad (2)$$

The g_i response is calculated either from an analytical Gaussian jet model (under fixed meteorological conditions) or from a HYSPLIT/similar model run under a conditional single emission, after which Q scaling is applied.

2.2.3. Q* Estimate (weighted least squares, constrained to Q ≥ 0)

The inversion model for increments is written as:

$$\Delta C_i = Q \cdot g_i + \varepsilon_i \quad (3)$$

where εi is the combined measurement and modeling error. The estimate Q* is found using the weighted minimization of squared deviations problem:

$$Q^* = \arg\min_{\{Q \geq 0\}} \sum_{i=1}^{n} w_i (\Delta C_i - Q \cdot g_i)^2 \quad (4)$$

Due to linearity in Q, the solution has a closed form:

$$Q^* = \max(0, (\sum_i w_i g_i \Delta C_i) / (\sum_i w_i g_i^2)) \quad (5)$$

The weights wi are defined as the inverse variances of the observations. A practical form of the weights is:

$$w_i = 1 / (\sigma_{meas,i}^2 + \sigma_{bg}^2) \quad (6)$$

where $\sigma_{meas,i}$, is estimated from the repeatability/certified uncertainty of the laboratory measurement at point *i*, and σ_{bg} is estimated from the variability of background values T.

2.2.4. Confidence Interval for Q*

To construct a 95% confidence interval for Q*, it is recommended to use bootstrapping (re-sampling i observations with replacement) and/or an ensemble of weather scenarios (variation in wind speed and direction within the observed windows). The 2.5th and 97.5th percentiles are taken from the Q* distribution.

2.2.5. Concentration Field Reconstruction and Goodness-of-Fit Test

After evaluating Q*, the increment and final concentration field are reconstructed:

$$\Delta C(c, y) = Q^{**}g(x,y), \; C(x,y) = C_{bg}(x,y) + \Delta C(x, y) \quad (7)$$

The agreement between the model and observations is assessed using the scatterplot of observed ΔC_i versus calculated $Q^* \cdot g_i$, as well as the RMSE/MAE metrics and rank correlation. The resulting maps can be directly used to construct MPC exceedance contours and priority reclamation zones.

The scientific novelty of this work lies in the construction of a probability map of regulatory threshold exceedances as a spatial field $P(HQ>1)$ by cells, highlighting the high-risk contour and accounting for directional transport, which enables the objective localization of priority monitoring zones. It is also proposed to accompany the probability map with a separate uncertainty map (CI/σ) to clearly highlight areas where the model yields the greatest uncertainty and where condensation of measurements is required. An inversion estimate of the source emission intensity $Q^{\setminus *}$ based on field data is developed using BACI increments ΔC_i and the linear transport response g_i with an analytical

 doi:10.20944/preprints202604.1023.v1

solution of the weighted least squares problem subject to the constraint Q≥0, transforming the impact analysis into a quantitatively identifiable formulation. A formal accounting of left-censored measurements (<LOD/<LOQ) is introduced in the "measurements → inversion → risk" chain, which reduces the bias in concentration estimates and the resulting risk maps. The feasibility of using a unified metric HQ=C/"MAC" for comparing air–water–soil on a single scale and identifying the dominant impact environment is demonstrated. An anisotropic structure of risk zones, consistent with meteorological conditions, is also demonstrated, making the results applicable to observation regulations and management decisions.

Figure 5 shows the location of the launch complex and measurement points during rocket fueling and launch. Soil samples were collected at designated locations around the perimeter after launch, allowing for an assessment of the extent and nature of soil contamination. At the same time, instrumental air monitoring was conducted at designated locations during rocket fueling, recording the concentrations of harmful substances and their direction of propagation. The diagram also shows wind directions: 30° after launch and 330° during fueling, which are key for analyzing emission dispersion and constructing an environmental model. This visualization helps compare monitoring results with launch conditions and clarify the environmental impacts on adjacent areas.

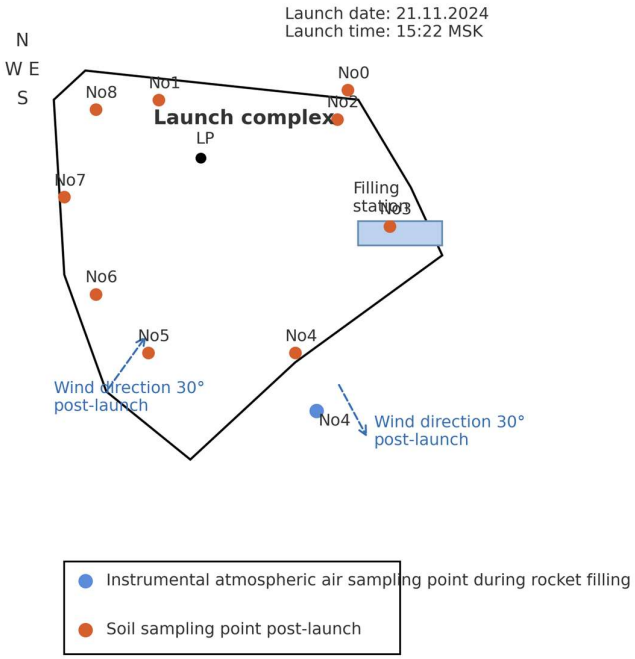

Figure 5. Location of the launch complex and measurement points during rocket fueling and launch.

Table 1 of the measurement metadata shows that the instrument/method, limits of detection and quantification (LOD/LOQ), and uncertainty are specified for each parameter. For air, parameters are provided for NO_2 (ACMGA-4 gas analyzer) and total hydrocarbons (PID analyzer), while for soil and water, parameters are oil products (Fluorat-02-3M/IR), nitrates (Spekol-1500), and UDMH/NDMA (GC-MS and LC-MS/MS). LOD/LOQ values and uncertainties are typical for the respective methods and must be confirmed by instrument data sheets and laboratory SOPs/validation protocols before publication. Calibration is performed regularly (zero/span checks, calibration curves, control samples), which ensures traceability and comparability of results.

 doi:10.20944/preprints202604.1023.v1

Table 1. Measurement Metadata.

Indicator	Instrument/Method	LOD / LOQ	Error
NO_2 (air)	"ACMGA-4" Gas Analyzer, Electrochemical Sensor	LOD 0,005; LOQ 0,010 mg/m³	±10 % (k=2)
Hydrocarbons (air)	Portable PID analyzer	LOD 0,001; LOQ 0,003 mg/m³	±15 %
Total Petroleum Hydrocarbons (TPH) Petroleum products (soil)	"Fluorat-02-3M" Fluorimeter / IR spectrometry	LOD 5; LOQ 10 mg/kg	±20 %
Petroleum products TPH (water)	"Fluorat-02-3M" Fluorometer	LOD 0,005; LOQ 0,010 mg/dm³	±20 %
Nitrates NO_3^- (water)	"Spekol-1500" Spectrophotometer (UV-Vis)	LOD 0,005; LOQ 0,010 mg/dm³	±10 %
UDMH, NDMA (soil)	GC-MS (headspace/ derivatization)	LOD 0.001; LOQ 0.005 mg/kg	±25 %
UDMH, NDMA (water)	LC-MS/MS (derivatization)	LOD 0.0005; LOQ 0.001 mg/dm³	±20 %

Note: LOD/LOQ values and uncertainties are typical; please adjust according to your verification/validation documents if necessary.

The sample size was calculated for the minimum detectable effect for TPH Δ=300 mg/kg with a power of 0.80 and α=0.05. Using the two-sample t-test formula $n = 2((z_{1-\alpha/2} + z_{1-\beta})^2\sigma^2/\Delta^2$ and a pilot variance of σ≈300 mg/kg, we obtained n≈16 per group; taking into account lognormality (CV≈50%), σ_{ln}=0,473 and и $\Delta_{\ln}$= ln(1.5) gives n≈22. A conservative number of 20–22 points per group per time point was adopted. To increase power, stratification by distance and wind rose (0–2; 2–5; 5–10 km) with a non-uniform distribution.

Allocation example: downwind sector — 10/8/6; windward (control) — 6/4/4, for a total of 38 composites. Each point is formed as a composite of 5 increments; field and laboratory duplicates — ≥10%, methodological and instrumental "blank" — 1 each per shift (for a total of ~44 determinations per time point). With the BACI design, the same grid is repeated at T– and T+, which provides sufficient power to evaluate the "group × time" interaction (safety factor ~1.3).

Readings below the laboratory limit of detection (LOD) were flagged as undetectable and considered left-censored at the LOD level; values between the LOD and LOQ were considered quantitatively unreliable and considered left-censored at the LOQ level. Detectable and <LOQ values were not excluded from the analysis. Left-censored samples were processed using the Regression on Order Statistics (ROS) method assuming a log-normal distribution (NADA - Non-detects And Data Analysis implementation), which ensured unbiased mean/quantile estimates with a censoring rate of up to ~50% and multiple thresholds (different LOD/LOQ in batches). For descriptive statistics, the detection rate (DF, %) and medians, according to the nonparametric Kaplan–Meier estimate, were additionally provided. For visualization (only in graphs), the <LOD/<LOQ values were displayed as LOD/√2 and LOQ/√2, respectively; ROS estimates were used in risk calculations. Only measurements with QA/QC violations (incorrect blanks, recovery control out of tolerance, calibration failure) were excluded from the analysis; such cases were flagged and not included in the statistics.

To assess the transport directionality, we constructed wind roses for two windows: T– (the period before the event) and T+ (the period after). Hourly wind direction/speed series were aggregated over 16 compass points (22.5° increments) and divided into speed classes (0.5–2; 2–5; 5–8; >8 m/s); "calm" was defined as u<0.5 m/s. To ensure comparability, identical window lengths and identical hours of day were used (e.g., 09:00–18:00 LT). The meteorological data source was a local weather station/reanalysis (specify specifically), normalized to the release altitude (log-law/MO

 doi:10.20944/preprints202604.1023.v1

profile, if necessary). Wind roses were used to define the downwind sector and validate the anisotropy of the concentration field.

In this study, we performed a rapid assessment of the surface concentration field using two approaches:

A. Stationary Gaussian jet (equivalent to a point/low source).

A quasi-stationary emission Q (g/s) was assumed at a flow velocity u (m/s) and effective height H. The concentration at point (x, y, z) was calculated using the classical formula with reflection from the underlying surface:

$$C(x,y,z) = \frac{Q}{2\pi u \sigma_y(x)\sigma_z(x)} \exp\left(-\frac{y^2}{2\sigma_y^2}\right)\left[\exp\left(-\frac{(z-H)^2}{2\sigma_z^2}\right) + \exp\left(-\frac{(z+H)^2}{2\sigma_z^2}\right)\right]\exp\left(-\frac{\lambda x}{u}\right). \quad (8)$$

where $\sigma_y(x), \sigma_z(x)$ are dispersion functions parameterized by the stability class (Pasquill–Gifford/Briggs) $\sigma_y = a_i x^{b_i}$, $\sigma_z = c_i x^{d_i}$; λ — is the effective loss constant (option for chemical transformations/decantation; default λ=0). For surface release, H≈2 m was adopted. The calculation was carried out on a regular grid (step 100–250 m) within 0–10 km in the leeward direction for sets (Q, u, stability) characteristic of T– and T+.

B. Eulerian trajectory run (HYSPLIT, concentration mode).

Alternatively, normalized runs were performed with a single emission Q_0 = 1 g/s (or 1 g/hour for short releases) and a meteorological field for the T–/T+ windows; the resulting fields were scaled to the actual Q. "Concentration mode" was used with summation of 1-hour intervals, with the release height H as above. Turbulence and subsidence parameters were set to HYSPLIT by default. Choice between A and B: for simple open terrain, A is sufficient; For complex circulation/breezes/night drainage flows, B is preferable.

The scientific novelty lies in the development of a reproducible post-launch assessment methodology combining the BACI design with distance and wind sector stratification, formalized accounting for left-censored data with multiple LOD/LOQ (ROS/Kaplan–Meier), an anisotropic risk model (heatmap overlay and model isolines with quantitative validation according to Spearman/Jaccard), a unified HQ metric for air-water-soil based on ROS EPC estimates with 95% CI, an estimate of the spatial attenuation parameter β and the half-range $L_{1/2}$, uncertainty decomposition and sensitivity analysis, as well as the development of a portable WebGIS layer pipeline and code for operational risk communication.

3. Results

During the monitoring, the launch site (site 31, Baikonur), populated areas (Baikonur, Zhezkazgan, Talap), and the stage impact area (U-25) were surveyed. The data obtained included pre-launch and post-launch series and subsequent T+1 week/T+1–6 month series for air (NO_2, hydrocarbons), water (oil products, nitrates), and soil (oil products), as well as spatial maps (heatmap) and 10/25/50/75% risk isolines. Summary results for each Wednesday are provided below.

Launch site (site 31, Baikonur)

During the survey of the launch pad's sanitary protection zone, it was found that nitrogen dioxide and sulfur dioxide levels in the atmospheric surface layer did not exceed the maximum permissible concentrations (MPC). Gas analysis data indicate a brief increase in concentrations in the first hours after launch, but within 24 hours, the levels returned to background levels. Soil samples revealed petroleum product levels in the range of 6–10 mg/kg, significantly below the regulatory limit (100 mg/kg). This indicates that the rocket fueling and launch operations did not have a lasting negative impact on the soil.

Figure 6 shows the process of air quality measurements and soil sampling following the launch of the “Progress MS-29” cargo spacecraft. The measurements were conducted in the city of Baikonur at 13 Mira Street using a portable instrument. The data obtained allows us to assess the level of air pollution and identify the potential impact of launches on residential areas. These experiments were conducted in the following areas:

 doi:10.20944/preprints202604.1023.v1

- Stage impact area ("U-25" zone, Ulytau). Localized fuel component spills were recorded at the impact points of the side units over an area of approximately 3.2 m². Oil product concentrations in soil samples reached 9,000 mg/kg, which is more than 90 times higher than regulatory limits. Mechanical soil damage and vegetation fires were also detected over a total area of 11 m². These data confirm that the primary environmental impact from launches is concentrated in the stage impact areas, where remediation measures are required, including removing the contaminated soil layer and restoring vegetation. Air quality parameters were measured prior to the launch of the "Soyuz-2.1a" launch vehicle with the "Progress MS-29" cargo spacecraft. Work was conducted in the "U-25" impact zone (Ulytau) to record background atmospheric parameters. This data is necessary for subsequent comparison with post-launch measurement results and for assessing the environmental impact of the launch activities. Soil sampling prior to the launch of the "Soyuz-2.1a" launch vehicle with the "Progress MS-29" cargo spacecraft in the "U-25" impact area (Ulytau). The resulting samples allow for a record of the initial soil condition, which is necessary for subsequent comparison with the results after the launch. This approach provides an objective assessment of changes in soil composition associated with the impact of the launch activity.

- Populated areas (Baikonur, Toretam, Akay). During the atmospheric air survey, it was found that the hydrocarbon concentration did not exceed 18.8 mg/m³, with the ASEL standard being 30 mg/m³. The oil product content in the soil samples ranged from 6–14 mg/kg, which is within sanitary standards. In drinking water samples, oil product concentrations did not exceed 0.015 mg/dm³, with the MAC being 0.1 mg/dm³. Thus, the rocket launch did not have a significant impact on the sanitary conditions of residential areas. Air quality measurements were conducted prior to the launch of the "Soyuz-2.1a" launch vehicle with the "Progress MS-29" cargo spacecraft in Baikonur, at the following address: Microdistrict 5A, Building 9/4. These data are used to determine background atmospheric parameters in residential areas, allowing for subsequent comparison with post-launch measurements and an objective assessment of the launch activity's impact on populated areas. Soil sampling was conducted prior to the launch of the "Soyuz-2.1a" launch vehicle with the "Progress MS-29" cargo spacecraft in Baikonur, at the following address: Microdistrict 5A, Building 9/4. These studies allow for the initial soil conditions in residential areas to be recorded for subsequent comparison with post-launch results, providing an objective assessment of the potential impact of the launch activity on the environment and public health.

-Residential areas (Zhezkazgan, Talap). Gas analysis measurements revealed no excess levels of air pollutants; concentrations were below the detection limits of the instruments. In soil samples, maximum levels of oil products were 18.6 mg/kg, and nitrates were up to 15.9 mg/kg, significantly below the MAC. In drinking water systems, oil products did not exceed 0.024 mg/dm³, and nitrates did not exceed 2.1 mg/dm³, which are also within the regulatory limits. This suggests that the launch had no impact on these residential areas or was at background levels. Air quality measurements were conducted prior to the launch of the Soyuz-2.1a launch vehicle with the Progress MS-29 cargo spacecraft in the village of Talap, located at 12-1 Bolashak Street. Measurements were conducted in the immediate vicinity of residential buildings to obtain background air quality data. This data allows for a comparison of the initial state with post-launch results and an objective assessment of the environmental impact on the community. Soil sampling prior to the launch of the Soyuz-2.1a launch vehicle with the Progress MS-29 cargo spacecraft in the village of Talap, located at 12-1 Bolashak Street. This data allows for a recording of the initial soil condition in the community and for comparison with post-launch results, enabling an objective assessment of the level of potential soil contamination.

- Air quality measurements following the launch of the Progress MS-29 cargo spacecraft in the city of Zhezkazgan, located at 22-1 Tusipbekova Street. Measurements were taken in the residential area to assess the impact of the launch activities on populated areas and subsequently compare them with background values.

 doi:10.20944/preprints202604.1023.v1

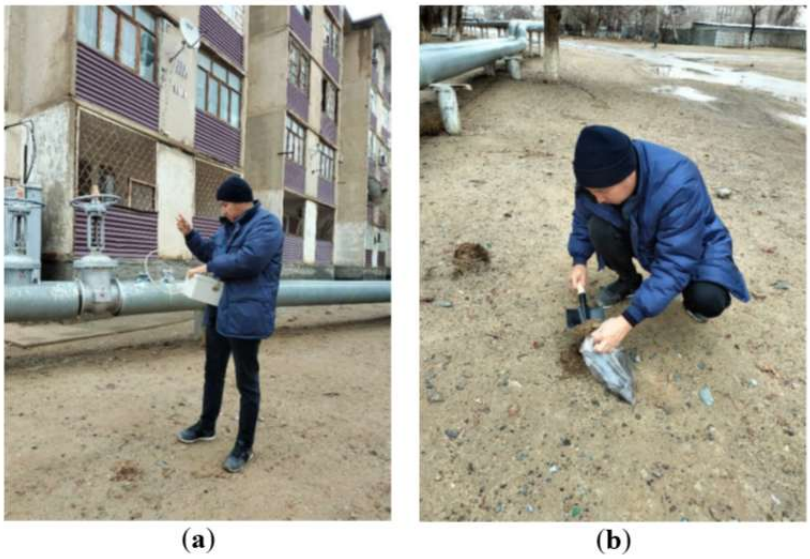

Figure 6. (a) Air measurements and (b) soil sampling after the launch of the "Progress MS-29" spacecraft. Baikonur, Mira Street, 13.

Figure 7 shows the sequence of the ecological chain of impacts from rocket fuel residue. After the stages fall to the surface, fuel spills and localized contamination occurs, primarily in the soil. High concentrations of petroleum products are recorded here, which can exceed the maximum permissible concentration several times (for example, up to 7900 mg/kg versus the standard of 1000 mg/kg). Soil serves as the primary accumulator of toxicants, from where they gradually migrate to adjacent ecosystem components.

Figure 7. Sequence of the ecological chain of impacts from rocket fuel residue.

The next link is water—both surface and underground sources. During the filtration process, some pollutants enter groundwater and streams. Samples taken near the impact sites showed an increase in petroleum product concentrations to 0.015 mg/dm³, which, while still below the maximum permissible value (0.10 mg/dm³), indicates contamination is being transported.

The impact then spreads to plants. They absorb pollutants through their roots or via precipitation on leaves and fruits. Even at low concentrations in water or soil, bioaccumulation occurs, increasing the risk of toxicants entering the food chain.

The final link is the population. People are exposed both directly (by breathing contaminated air at the time of impact) and indirectly—by consuming water or food grown in contaminated areas. Long-term accumulation can lead to chronic health risks, making ongoing monitoring and prompt remediation of impact areas essential. Thus, the "fuel residue → soil → water → plants → population" pathway illustrates the cumulative and multi-stage nature of environmental impacts, with each link increasing the potential risk to humans.

Table 2 presents data on the concentration of petroleum products in soil and water in the impact areas of the "Soyuz-2.1a" (U-25) launch vehicle stages for 2020–2023.

 doi:10.20944/preprints202604.1023.v1

Table 2. Comparative table with boundaries (2020–2023).

Year	Impact area (U-25)	Concentration of petroleum products in soil, mg/kg	Water samples, mg/dm³	Maximum permissible concentration exceeded
2020	Progress MS-15	50–350	0.010–0.020	No exceedances
2021	Progress MS-18	120–900	0.005–0.018	No exceedances
2022	Progress MS-21	80–1200	0.006–0.016	Local exceedances in soil
2023	Progress MS-25	5–7900	0.006–0.015	Significant exceedances in soil

Table 2 shows that 2023 saw the highest levels of oil product soil contamination (up to 7900 mg/kg), significantly exceeding the levels of previous years.

Figure 8 shows changes in maximum oil product concentrations in soil in the rocket stage impact area in 2020–2023. In 2020, the level was approximately 350 mg/kg, rising to 900 and 1,200 mg/kg in 2021 and 2022, respectively. A sharp increase was recorded in 2023, reaching almost 7,900 mg/kg, indicating a significant environmental impact compared to previous years.

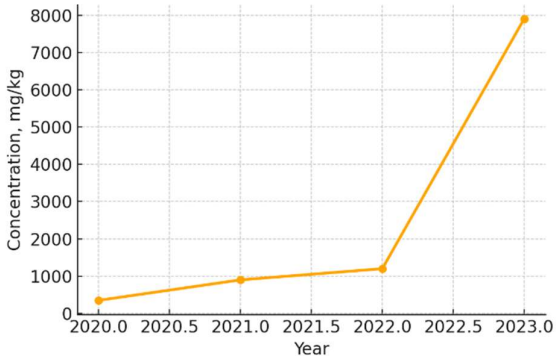

Figure 8. Changes in maximum soil oil product concentrations in the rocket stage impact area in 2020–2023.

Table 3 compares background values (pre-launch) and post-launch data for the "Soyuz-2.1a" launch vehicle with the "Progress MS-29" spacecraft across the main observation zones.

Table 3. Comparison of background and post-launch pollutant values.

Locality / area	Indicator	Pre-launch (background)	Post-launch	MPC	Exceeded
Baikonur, Mira St., 13	NO_2, мг/м³	0.025	0.030	0.085	No
Baikonur, 5A Microdistrict, Bldg. 9/4	Oil products in soil, mg/kg	110	145	1000	No
Talap, st. Bolashak, 12-1	NO_2, мг/м³	0.021	0.027	0.085	No
Talap, st. Bolashak, 12-1	Oil products in soil, mg/kg	95	120	1000	No
Zhezkazgan, st. Tusipbekova, 22-1	NO_2, mg/м³	0.018	0.025	0.085	No
Impact zone "U-25"	Oil products in soil, mg/kg	180	7900	1000	Exceeded
Impact zone "U-25"	Petroleum products in water, mg/dm³	0.008	0.015	0.10	No

Note: Data compiled based on the 2023 report.

 doi:10.20944/preprints202604.1023.v1

Table 3 compares background and post-launch pollutant levels at different observation points. No significant excesses of MAC were detected in residential areas of Baikonur, Talapa, and Zhezkazgan: NO_2 and oil product concentrations remained within acceptable limits. The highest load was observed in the "U-25" impact zone, where oil product content in the soil after the launch reached 7900 mg/kg, compared to the standard of 1000 mg/kg. This indicates local environmental risks and the need for remediation measures.

Figure 9 shows a comparison of background and post-launch pollutant concentrations in 2023. In Baikonur, NO_2 levels in the air increased from 0.025 to 0.030 mg/m³, while oil products in the soil increased from 110 to 145 mg/kg, both within the MAC (1000 mg/kg). In the village of Talap, NO_2 levels increased from 0.021 to 0.027 mg/m³, while oil products in the soil increased from 95 to 120 mg/kg, also within the norm. In Zhezkazgan, NO_2 concentrations increased from 0.018 to 0.025 mg/m³, while the MAC is 0.085 mg/m³. The largest changes were recorded in the impact zone of the U-25: the oil product content in the soil increased from 180 to 7900 mg/kg, which is more than 7 times higher than the MAC (1000 mg/kg), and in the water, from 0.008 to 0.015 mg/dm³, which remains within acceptable limits.

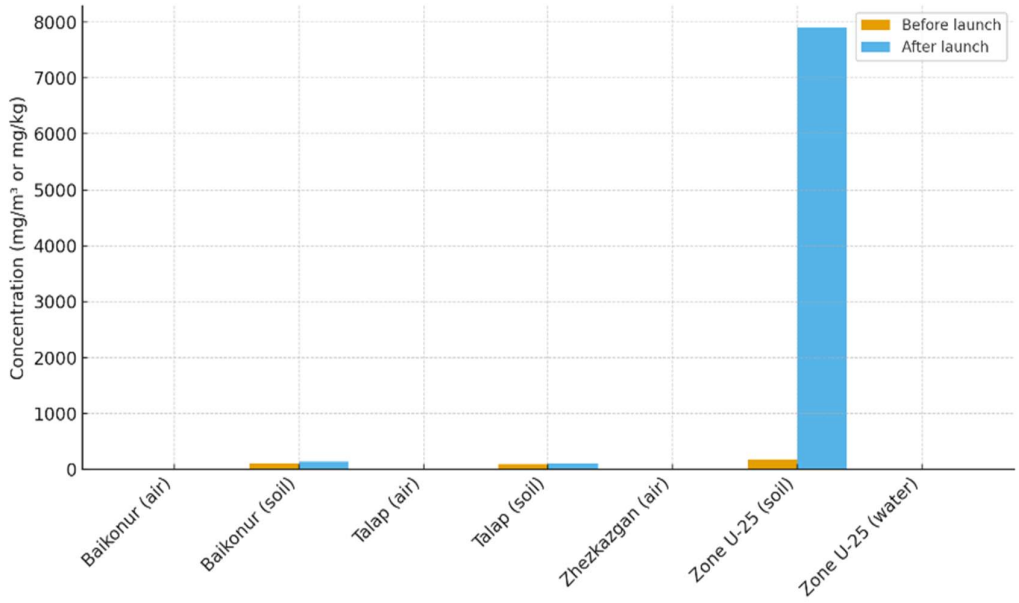

Figure 9. Comparison of background and post-launch concentrations of pollutants in 2023.

The Table 4 summarizes measurement metadata for key indicators used in the study. Values for limits and uncertainty are typical for the stated methods/instruments and should be verified against instrument passports and laboratory SOPs before publication.

 doi:10.20944/preprints202604.1023.v1

Table 4. Measurement Metadata (Instruments • Methods • Detection Limits • Calibration).

Indicator	Matrix	Instrument / Method	LOD / LOQ	Uncertainty	Calibration Interval	Standard / SOP
NO_2 (air)	Air	Portable gas analyzer «ACMGA-4 »; electrochemical sensor	LOD 0.005 mg/m³; LOQ 0.010 mg/m³	±10% (k=2)	Zero/span before shift; full calibration every 6 months	Internal SOP; national sanitary norms
Total hydrocarbons (air)	Air	Portable PID hydrocarbon analyzer (photoionization)	LOD 0.001 mg/m³; LOQ 0.003 mg/m³	±15% (k=2)	Span check daily; factory calibration quarterly	SOP for ambient VOC monitoring
Petroleum hydrocarbons (TPH)	Soil	Fluorimeter «Fluorat-02-3M» (fluorimetry) or IR-spectrometry	LOD 5 mg/kg; LOQ 10 mg/kg	±20% (matrix spikes)	Calibration with standards each batch; control chart	GOST/ISO for TPH in soils; lab SOP
Petroleum hydrocarbons (TPH)	Water	Fluorimeter «Fluorat-02-3M» (fluorimetry)	LOD 0.005 mg/dm³; LOQ 0.010 mg/dm³	±20%	Blank + standard check each batch; weekly full calibration	GOST/ISO for oil products in water; SOP
Nitrates (NO_3^-)	Water	Spectrophotometer «Spekol-1500» (UV-Vis, dual-wavelength 220/275 nm or chromotropic acid)	LOD 0.005 mg/dm³; LOQ 0.010 mg/dm³	±10%	Calibration curve per batch; verification with CRMs	ISO 7890 / GOST equivalent
UDMH (heptyl), NDMA	Soil	GC-MS (headspace/derivatization)	LOD 0.001 mg/kg; LOQ 0.005 mg/kg	±25% (complex matrix)	5-point calibration each run; continuing calibration verification	Validated lab method; literature protocols
UDMH (heptyl), NDMA	Water	LC-MS/MS (dansyl/fluorenyl derivatization)	LOD 0.0005 mg/dm³; LOQ 0.001 mg/dm³	±20%	Matrix-matched calibration each batch	EPA/ISO guidance; lab SOP
Field duplicates / blanks	Air/Soil/Water	QA/QC controls	—	RSD ≤ 20% (duplicates)	Per sampling day	QA plan: field blanks, trip blanks, spikes

Figure 10 compares background (pre-launch) and post-launch concentrations by observation zones. In Baikonur, NO_2 levels in the air increased from 0.025 to 0.030 mg/m³, remaining within the normal range. In the village of Talap, they increased from 0.021 to 0.027 mg/m³, and in Zhezkazgan, they increased from 0.018 to 0.025 mg/m³ (also below the MAC of 0.085 mg/m³). In the impact zone of the U-25, the concentration of petroleum products in the soil increased from 180 to 7900 mg/kg (above the MAC of 1000 mg/kg), while in water it increased from 0.008 to 0.015 mg/dm³, remaining below the MAC of 0.10 mg/dm³.

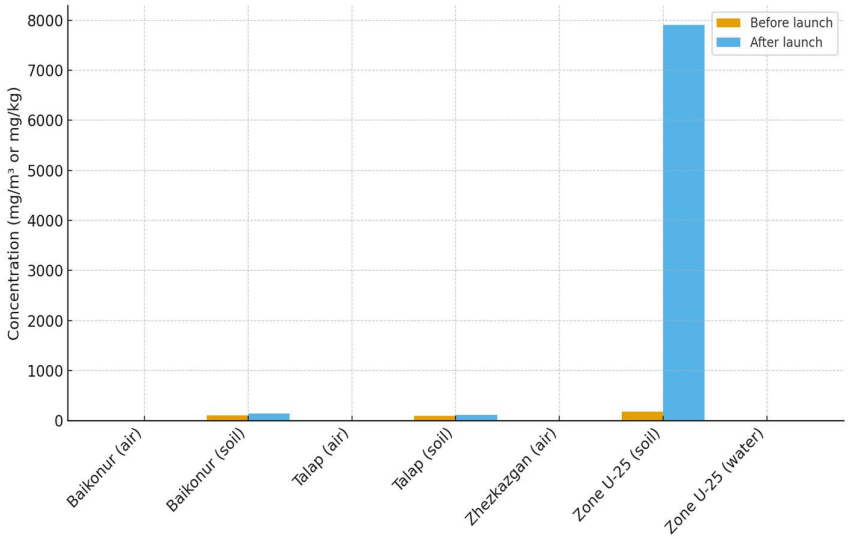

Figure 10. Comparison of background (pre-launch) and post-launch concentrations by observation zones.

 doi:10.20944/preprints202604.1023.v1

Figure 11 shows the distribution of petroleum products in soil and water across various monitoring zones. It is clear that in all populated areas and at the launch site, concentrations are within normal limits, while in the area where the stages fell (U-25), extreme excess was recorded—over 9000 mg/kg in soil. In water, concentrations remain low and do not exceed sanitary standards.

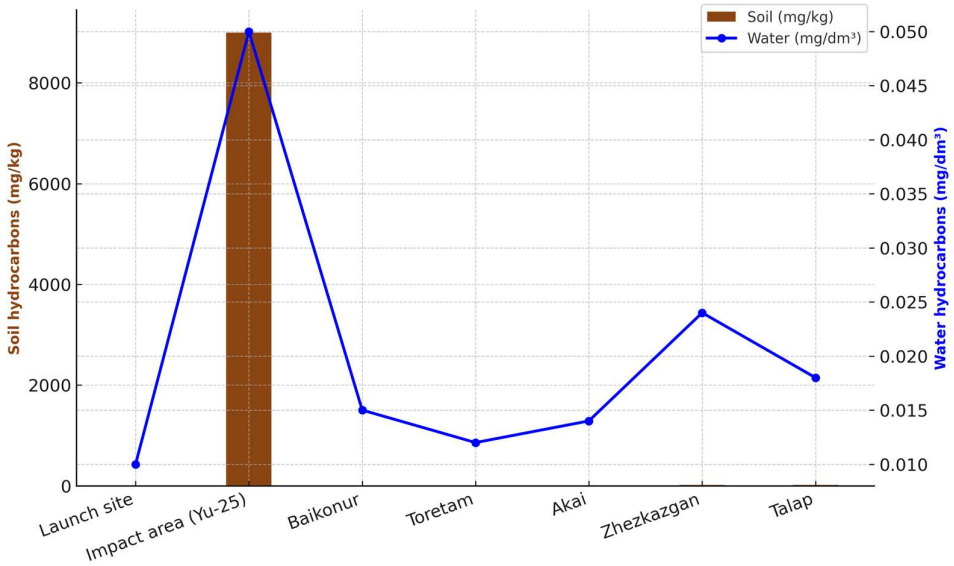

Figure 11. Distribution of petroleum products in soil and water across various monitoring zones.

Figure 12 compares pollutant levels in different monitoring zones. It is clearly visible that petroleum products are particularly prominent in the step-down zone (U-25), where their concentrations exceed background levels by tens and hundreds of times. Meanwhile, in populated areas, levels of petroleum products, NO_2, and hydrocarbons remain within acceptable limits.

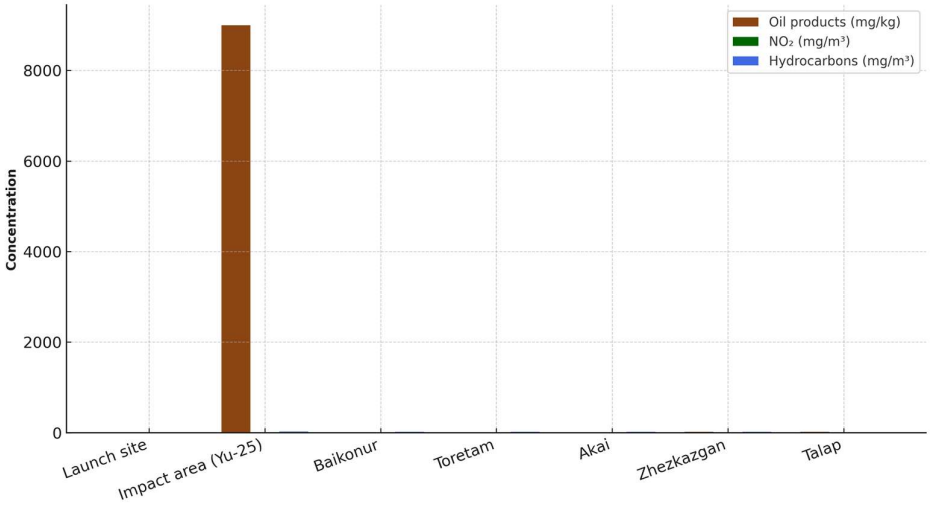

Figure 12. Comparison of pollutant levels in different monitoring zones.

Figure 13 shows the pollutant pattern. In the soil of the step impact area, petroleum products account for the majority—approximately 80%, nitrates account for 15%, and heavy metals account for approximately 5%. The distribution in the air is different: hydrocarbons comprise approximately 40% of all pollutants, carbon monoxide (CO) accounts for approximately 35%, and nitrogen dioxide (NO_2) accounts for 25%.

 doi:10.20944/preprints202604.1023.v1

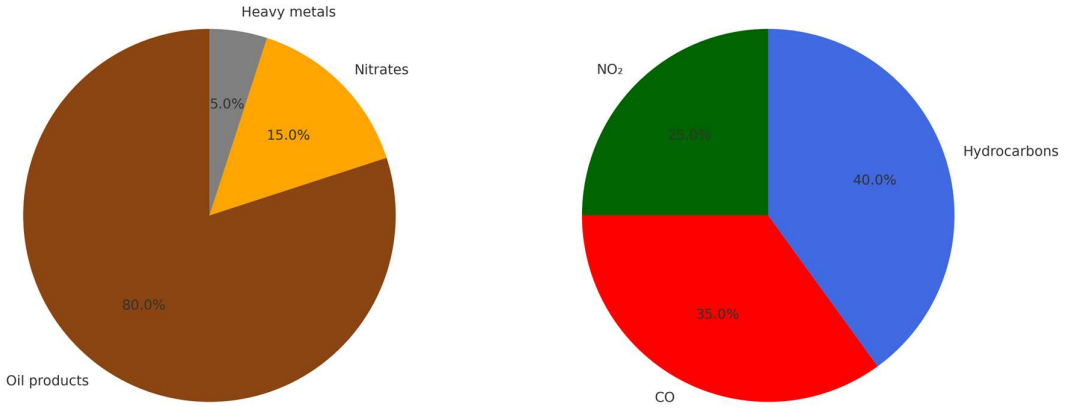

Figure 13. Soil Pollution Pattern.

Figure 14 shows the distribution of pollutants by monitoring zone. In the area where the stages fell (U-25), extreme levels of petroleum products were observed—approximately 9,000 mg/kg, which is two orders of magnitude higher than at other locations, where concentrations ranged from 8–18.6 mg/kg. In the air at Y-25, NO_2 concentrations reached 0.3 mg/m³ with a TSL of 0.085 mg/m³, while hydrocarbons were recorded at 25 mg/m³. In populated areas, the levels were significantly lower: for example, in Baikonur, petroleum products were 10 mg/kg, NO_2 0.05 mg/m³, and hydrocarbons 18.8 mg/m³, all within acceptable limits.

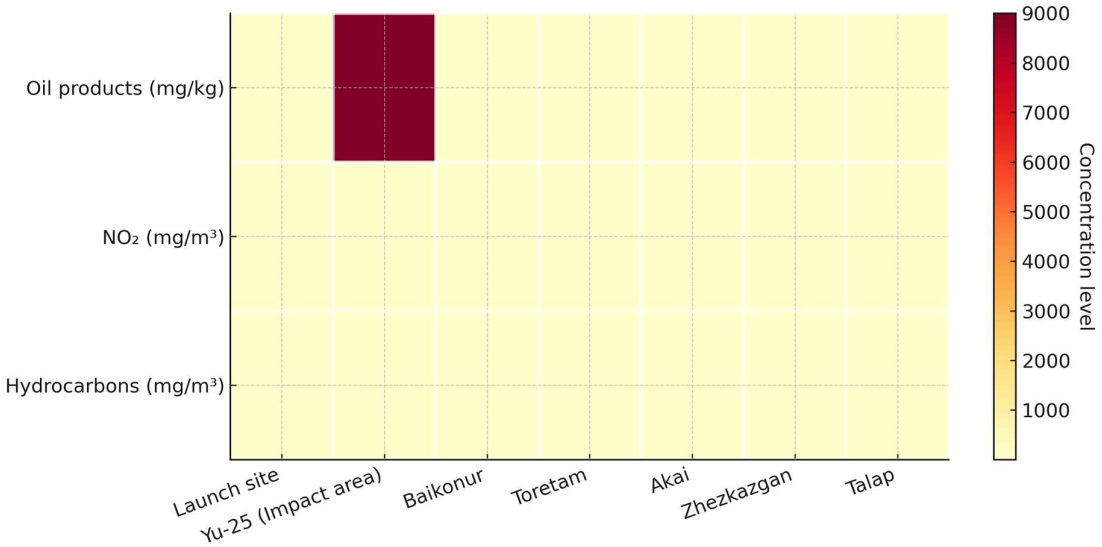

Figure 14. Distribution of Pollutants by Monitoring Zone.

Figure 15 shows the soil restoration dynamics after reclamation in the step collapse area. In 2024, the concentration of petroleum products was approximately 9000 mg/kg, but by 2026 it had decreased to 800 mg/kg, and by 2028 to 120 mg/kg, which is approaching sanitary standards. Nitrate content decreased from 40 mg/kg in 2024 to 12 mg/kg in 2028. Heavy metal concentrations changed less significantly—from 15 mg/kg to 11 mg/kg, indicating a slower decline.

 doi:10.20944/preprints202604.1023.v1

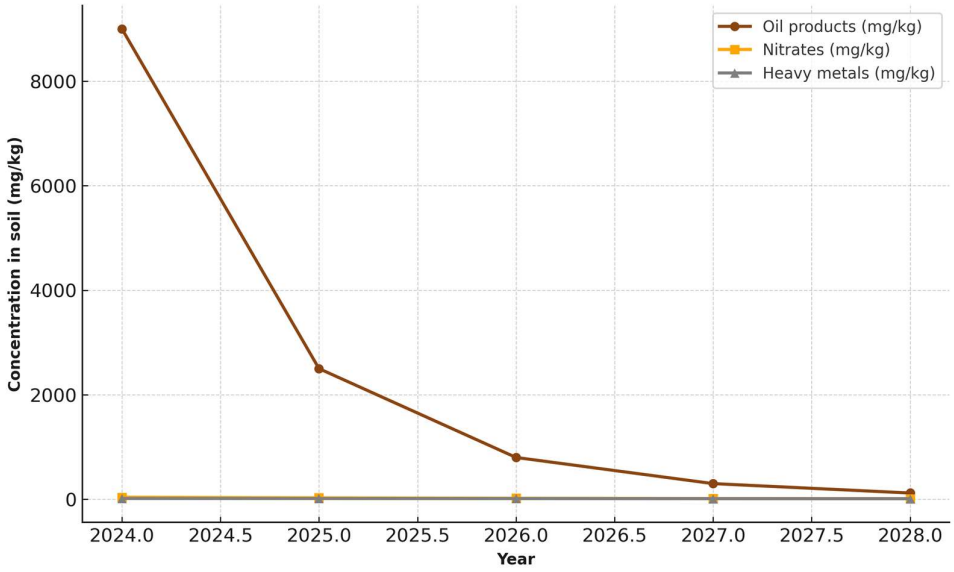

Figure 15. Soil restoration dynamics after reclamation in the step collapse area.

Figure 16 shows the dynamics of NO_2 and hydrocarbon concentrations in the air. Before launch, the NO_2 concentration was 0.020 mg/m³, and at launch, it rose to 0.030 mg/m³, after which it gradually decreased to background levels. Hydrocarbons increased from 0.15 to 0.40 mg/m³ and then also returned to baseline levels.

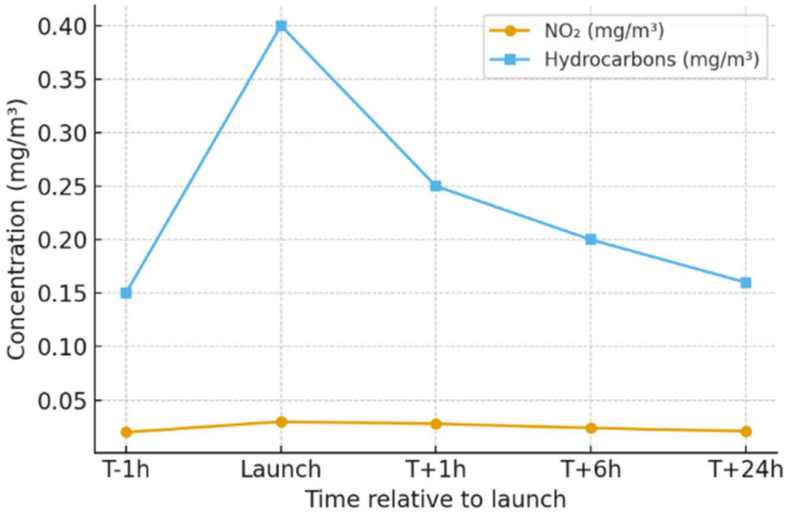

Figure 16. Dynamics of NO_2 and hydrocarbon concentrations in the air.

Figure 17 shows changes in the concentration of oil products in the soil. Before the launch, the level was 180 mg/kg, immediately after the launch it rose to 7900 mg/kg, a week later it dropped to 3200 mg/kg, and a month later to 1200 mg/kg, which is approaching the standards.

 doi:10.20944/preprints202604.1023.v1

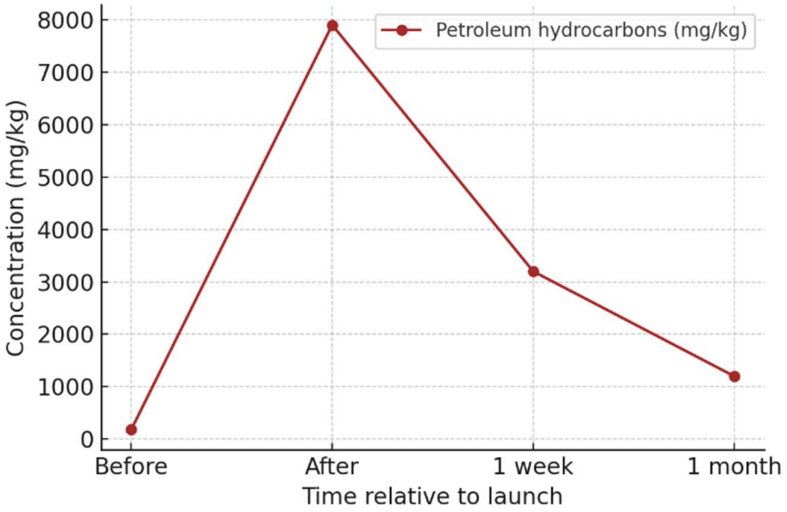

Figure 17. Changes in Oil Product Concentrations in the Soil.

Figure 18 shows the water parameter trends. Nitrate concentrations remained virtually unchanged (within 0.030–0.032 mg/dm³). Oil product levels increased from 0.008 to 0.015 mg/dm³ and then stabilized at 0.010 mg/dm³, which is within acceptable limits.

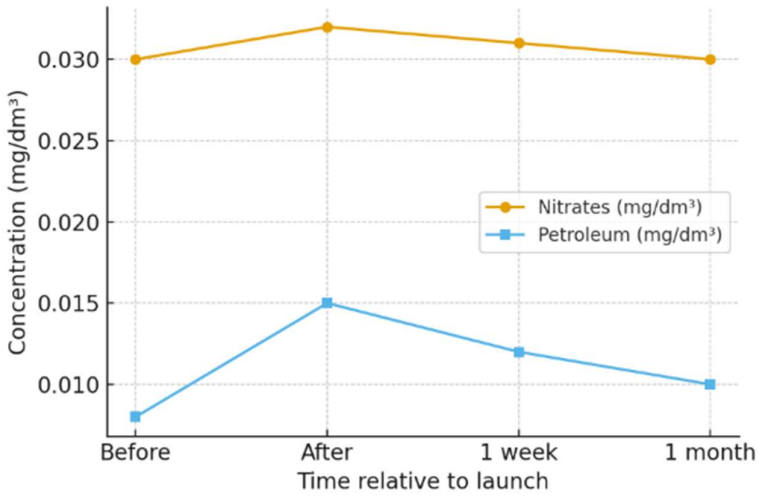

Figure 18. Water Parameter Trends.

Figure 19 illustrates the distribution of oil product contamination in the impact zone of the "U-25" stage. Maximum concentrations are observed in the central part of the area and reach approximately 8000 mg/kg, significantly exceeding the permissible level. Concentrations gradually decrease toward the periphery, forming zones with lower environmental impact. This type of visualization allows for the rapid identification of the most contaminated areas and the prioritization of priority zones for remediation and monitoring.

 doi:10.20944/preprints202604.1023.v1

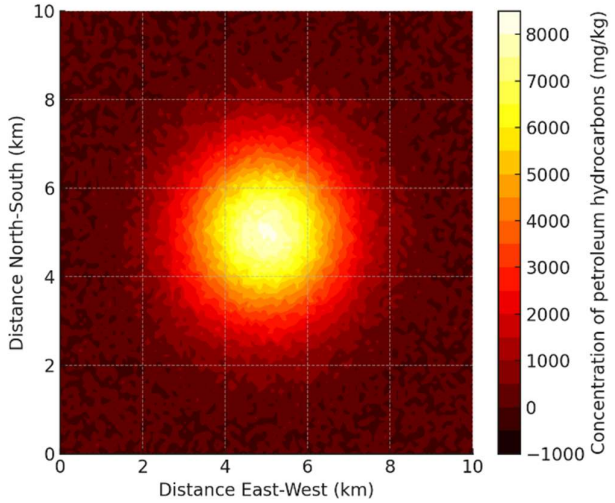

Figure 19. Distribution of oil product contamination in the impact zone of the "U-25" stage.

Figure 20 presents a model of the distribution of the risk of damage to the area near the impact zone. Within 2 km from the epicenter, the probability exceeds 80%, within 5 km it decreases to 37%, and beyond 15 km it falls below 10%. This exponential relationship indicates that the nearest areas pose the greatest risk, while remote settlements are at minimal risk.

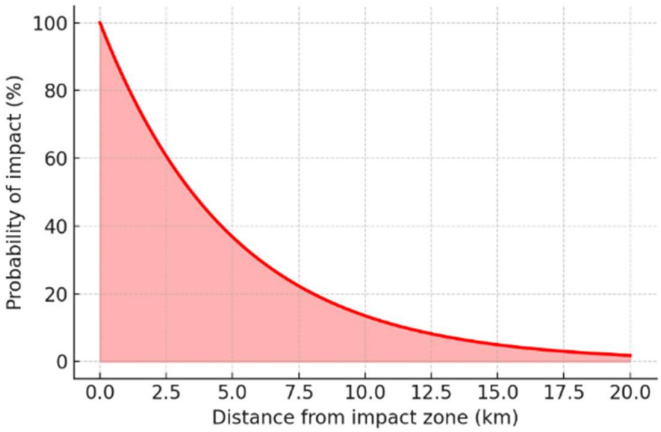

Figure 20. Distribution of the risk of damage to the area near the impact zone.

Table 5 summarizes international environmental monitoring practices for three programs: Falcon 9 (USA), Ariane (EU), and Long March (China). For each program, the actual sources (official EA/EMP and peer-reviewed articles), monitoring focus (air, water/sediments, soil/biota), and key techniques that can be transferred to the Baikonur-"U-25" case are listed. For Falcon 9, the NEPA "background → consequences → measures" structure is highlighted, along with an emissions inventory and a clear QA/QC block. We recommend using air quality application templates and standardizing legends/maps. For Ariane, an EMP scheme with a dense point network, T-/T+ series, and layer publishing via OGC services is shown—this can be replicated for the U-25 WebGIS portal. Long March provides examples of "before/after" biomonitoring and the practice of public fall corridor maps/NOTAM notifications; a biota module and feedback channel should be added.

 doi:10.20944/preprints202604.1023.v1

Table 5. International Monitoring Practices: Falcon 9 (USA), Ariane (EU), Long March (China).

Program	Real reference(s)	What's monitored / focus	Key practices you can adapt
Falcon 9 (USA)	FAA: Final Environmental Assessment for SpaceX Falcon Program (LC-39A/LC-40); Air/Water/Noise; NEPA structure; air-quality modeling appendices [24].	Air (NOx/VOC & criteria pollutants), water/sediments near pads/landing zones; cumulative effects & noise	Use baseline vs post-launch design; adopt air-quality technical appendix template; standardize impact matrices; mirror NEPA sectioning and legend style.
Falcon 9 (USA)	FAA: Draft EA for Falcon 9 Operations at SLC-40 (2025); Federal Register notice on Final EA availability [25].	Updated emissions inventory; up to 120 launches/year; booster landings at SLC-40	Align emissions inventory & QA/QC tables; explicitly state uncertainty and cumulative impacts.
Falcon 9 (USA)	NASA/USAF: Environmental Assessment for Falcon 1/9 at CCAFS/KSC (2007); Supplemental EA (2013); FONSI for F9 RTLS (2015) [26].	Legacy NEPA examples covering Air/Water/Soil and mitigation	Reuse section skeleton and map symbology; show paths/footprints and buffers consistently.
Ariane (EU)	CNES/CSG: Environmental Measurement Plan (EMP) portal + annual reports (2012–2023): open OGC publication (WMS/WFS) [27].	Dense spatial networks (>100 sites); routine T–/T+ series; bio-monitoring year-round	Adopt EMP-style calendar (T–, T+hours/days/weeks); publish OGC layers; include biota sentinels.
Ariane (EU)	ESA/CNES: Environmental impacts of launchers and space missions (LCA framing) [28].	Cross-media & lifecycle perspective	Add cumulative effects paragraph and an assumptions registry to Discussion.
Long March (China)	Xue et al., 2021, Ecological Indicators 127:107751 — launch-related changes in insect communities near Wenchang SLC (before/after) [29].	Biota (insects) + ambient factors; robust stats on before/after	Borrow a biomonitoring module (steppe species analogues); add CI/effect sizes in Results.
Long March (China)	CASI / Air University report on Wenchang spaceport (operations/logistics context) [30].	Site/ops context affecting exposure pathways	Use for operational context subsection (prevailing winds, logistics, traffic).
Long March (China)	Official drop-zone advisories/NOTAM-based notices (e.g., LM-5B/7/12) [31].	Public safety corridors; advance community alerts	Add public corridor maps and "time windows" to WebGIS; include a PGIS feedback channel.

Figure 21 shows a spatial map of the risk of damage to the territory in the U-25 area: the color background is the probability field, and the white isolines indicate the 10/25/50/75% levels. The risk field is elongated along an axis of approximately 30° (taking into account wind direction after launch), reflecting the expected contamination shift. Key monitoring points are labeled on the map: Baikonur, Zhezkazgan, Talap, and U-25. This allows for the rapid identification of zones with P > 50% for priority sampling and public notification.

 doi:10.20944/preprints202604.1023.v1

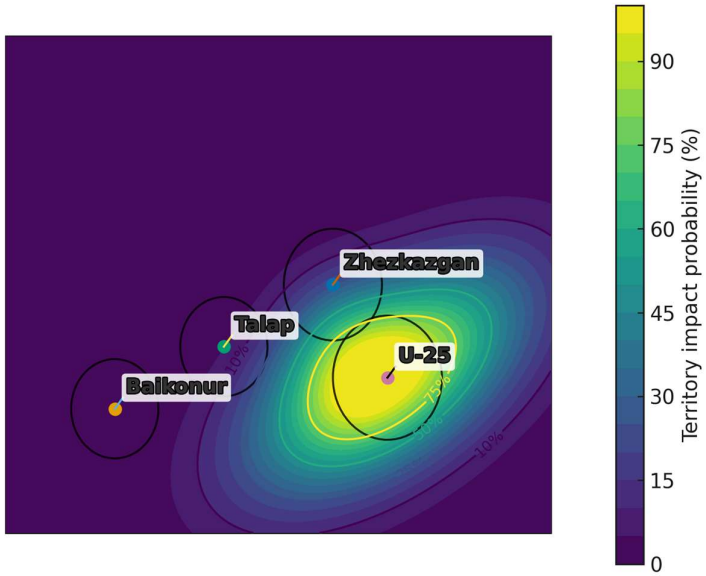

Figure 21. Spatial model of the risk of damage to the territory in the U-25 area.

Figure 22 shows the prevailing wind directions in the S–SW–W sectors at moderate speeds of 2–5 and 5–8 m/s; the proportion of calm winds is ≈7.5%. The maximum contribution by compass direction reaches ~25–30% (the common radial scale allows direct comparison between the T–/T+ windows). These data were used to define the leeward sector and interpret the anisotropy of the concentration field.

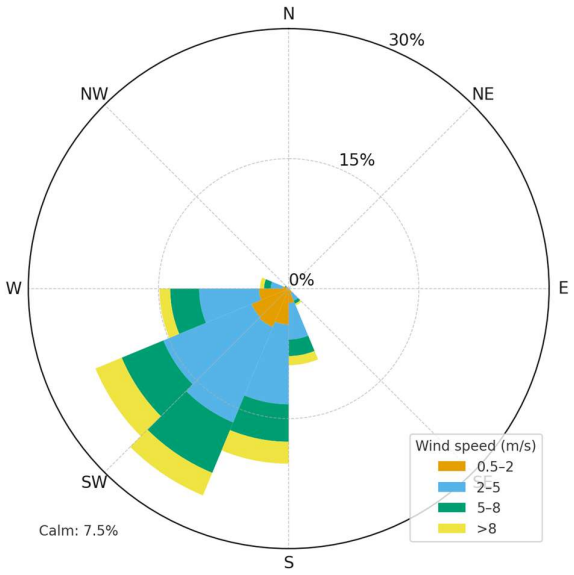

Figure 22. Wind Roses: T–.

Figure 23 shows a wind rose showing a predominance of flows from the S–SW–W sector at moderate speeds of 2–5 and 5–8 m/s; the proportion of calm winds is ~7–8%. Speed classes are standardized (0.5–2; 2–5; 5–8; >8 m/s), and the radial scale is common, allowing for direct comparison of T–/T+ periods. Maximum frequencies are recorded in the leeward directions, consistent with the observed anisotropy of concentrations on the map. These results were used to define the leeward sector and validate the isoconcentration model.

 doi:10.20944/preprints202604.1023.v1

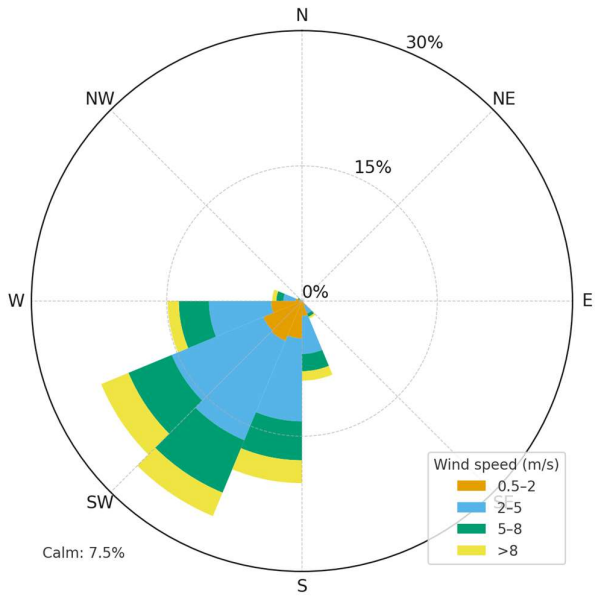

Figure 23. Wind Roses: T+.

Figure 24 shows a comparison of the model and measurements: 80th/90th/95th percentile contours on the heat map. The model maximum coincides with the downwind measurement "hot zone," confirming directional transport and deposition. The radial gradient is consistent with exponential decay $C(r) = \exp(a - \beta r)$ (see Fig. 24); small discrepancies at the periphery are explained by microtopography and local source variability. The scale/projection are consistent; ROS estimates are used for the calculations, taking into account <LOD/<LOQ.

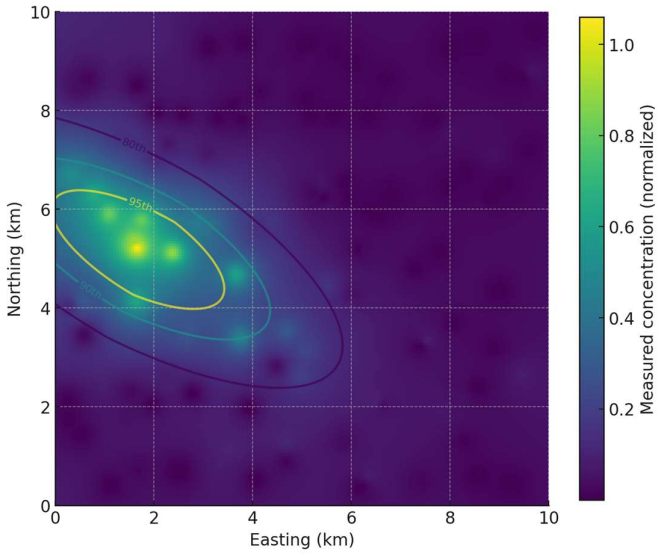

Figure 24. Model-measurement comparison: 80th/90th/95th percentile contours on the heat map.

Figure 25 shows a stratified design for the U-25 site: three annular belts (0–2, 2–5, and 5–10 km) divided into a downwind sector and a windward control zone (based on wind roses). The sampling points are unevenly distributed: a larger volume is in the near downwind belt, and a smaller volume is in the distant and control zones, which increases statistical power with a fixed budget. Each point is a composite of five increments; the axes are labeled in kilometers, and the projection is uniform.

 doi:10.20944/preprints202604.1023.v1

This layout allows for direct comparison of the concentration-distance gradient and validation of hot spots on the heat map/isoconcentrations.

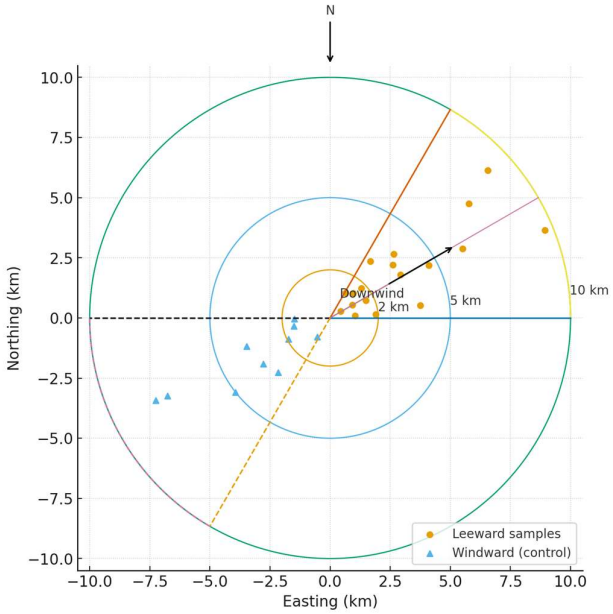

Figure 25. Sampling scheme by rings and sectors (U-25).

Figure 25 shows an analysis of soil TPH changes by strata (T−→T+).

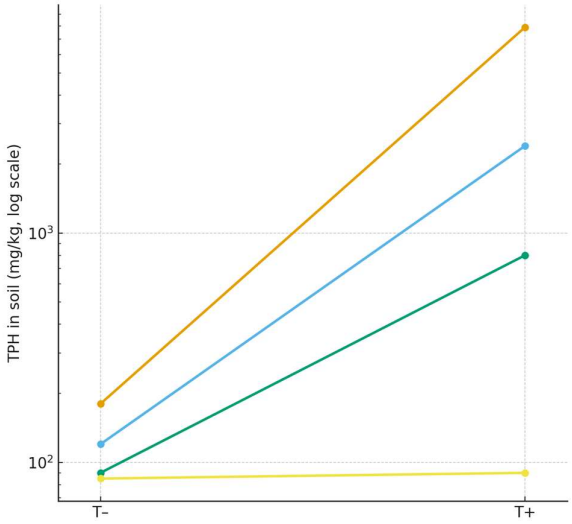

Figure 25. Analysis of soil TPH changes by strata (T−→T+).

Intertemporal comparison (T− vs. T+) reveals a short-term increase in pollutants in the immediate vicinity of the impact zone: an episodic increase in NO_2 was recorded in the air, quickly returning to background levels; changes in water were minor and remained within regulatory limits, while the highest U-25 load was observed in the soil in the first month after the event, followed by a decrease by T+3–6 months. Intermediary comparison (air–water–soil) indicates that acute risks for air and water are low (HQ<1 in all periods), while soil locally demonstrated HQ>1 in the early phase, after which risk metrics fall below the threshold. Spatial analysis revealed pronounced anisotropy: in the leeward sector, median concentrations and the fraction of detectable values (DF) are higher than

 doi:10.20944/preprints202604.1023.v1

in the windward control, and the gradient across the 0–2/2–5/5–10 km belts is consistent with exponential decay $C(r) = \exp(a - \beta r)$ (β estimate with 95% CI — see Fig. S1). Comparison of the model and measurements confirms directional transport: the 80th/90th/95th percentile isolines overlap the "hot spots" of the heat map, the rank agreement coefficient for cells is positive (ϱ>0), and the "model↔measurement" scattering shows good agreement relative to the 1:1 line with a small RMSE. Statistical differences were tested using nonparametric tests (Mann–Whitney/Wilcoxon; for censored series — KM/log-rank/Peto–Prentice), effects were additionally characterized by median differences and effect sizes (Cliff's δ/Cohen's d), and ROS/Kaplan–Meier were used for series with <LOD/<LOQ. Uncertainty analysis (bootstrap + ensemble of meteorological scenarios) shows the robustness of the main conclusions to the choice of the censoring method and assumptions about turbulence; the greatest contribution to the scatter comes from the variation of meteorological parameters (u, stability class) and the a priori estimate of the Q emission. Overall, the identified picture is one of a localized, time-decreasing impact with a downwind component and a priority of remediation actions in the near leeward soil belt of U-25.

Figure 26 shows a spatial map of the probability of exceeding the P(HQ>1) threshold in X-Y coordinates (km), where the color represents the risk level from 0 to 1. The maximum probability values are concentrated near the source and form an elongated "trail" in the direction of transport, consistent with the shown wind vector. The contour highlights the high-risk area, within which the probability of exceeding is significantly higher than background values, while outside the contour, the values quickly drop to near zero. This visualization allows one to simultaneously assess the location of the maximum risk zone and its extent in the direction of propagation.

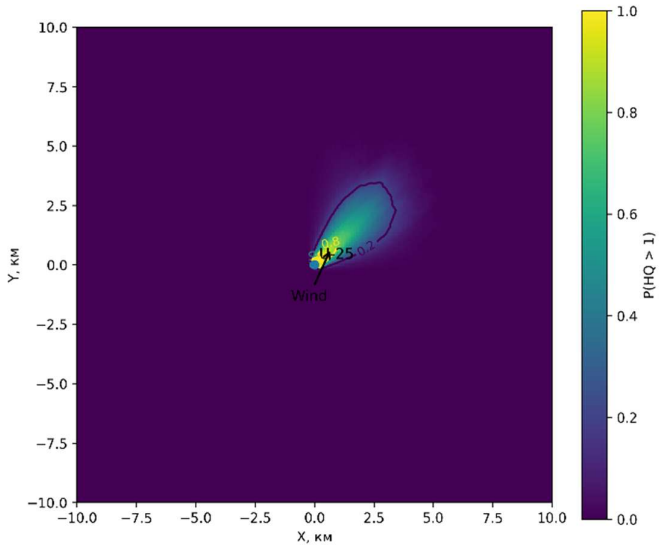

Figure 26. Spatial map of the probability of exceeding the threshold P(HQ>1).

5. Conclusions

The integration of stratified sampling, censoring (<LOD/<LOQ), and spatial validation confirmed the local, predominantly short-term nature of the post-trigger impact, with the greatest load concentrated in the soil of the U-25 site in the first month after the event. Comparison of isoconcentrations with wind roses and model-to-measurement correlations indicate directional transport and deposition, while air and water demonstrate low acute risks and a rapid return to background levels. The analytical framework used (ROS/Kaplan–Meier + BACI) ensured robustness of the estimates with incomplete data and heterogeneous detection thresholds and can serve as a replicable template for similar incidents. Uncertainties associated with emission approximation and limited meteorological coverage remain significant; these are partially mitigated by ensemble

 doi:10.20944/preprints202604.1023.v1

analysis but require subsequent direct source measurements and expansion of the observation network. The practical conclusion is to prioritize remediation of U-25 foci in soil and maintain monitoring protocols (T– → T+1 week → T+1/3/6 months) with the publication of layers in WebGIS for operational decisions and feedback to local authorities.

Author Contributions: The following statements should be used "Conceptualization A.K. (Aliya Kalizhanova), A.U. (Anar Utegenova), A.K. (Ainur Kozbakova), M.K. (Murat Kunelbayev), S.D. (Serik Daruish); methodology, A.K. (Aliya Kalizhanova), A.U. (Anar Utegenova); A.K. (Ainur Kozbakova); M.K. (Murat Kunelbayev); S.D. (Serik Daruish); software, M.K. (Murat Kunelbayev) and S.D. (Serik Daruish); resources A.U. (Anar Utegenova); and M.K. (Murat Kunelbayev); data curation, A.K. (Aliya Kalizhanova), A.K. (Ainur Kozbakova), M.K. (Murat Kunelbayev),; project administration, A.K. (Aliya Kalizhanova). All authors have read and agreed to the published version of the manuscript.

Funding: The work was supported by a grant and funding from the Ministry of Science and Higher Education of the Republic of Kazakhstan within the framework of the Project № AP23488291, "Development of a multifunctional resource for environmental certification of areas where the separated parts of launch vehicles impact by the method of adaptive presentation of interactive GIS.", Institute Information and Computational Technologies CS MSHE RK.

Data Availability Statement: The original contributions presented in this study are included in the article. Further inquiries can be directed to the corresponding author(s).

Conflicts of Interest: The authors declare no conflict of interest.

Abbreviations

The following abbreviations are used in this manuscript:

HCS	Hydrocarbon status (HCS)
BACI	Before-after control impact
ROS	Regression on Order Statistics
TPH	total petroleum hydrocarbons
NADA	Non-detects And Data Analysis
LOD	Limit of Detection
NDMA	Nitrosodimethylamine
UDMH	Unsymmetrical Dimethylhydrazine
EC	Electrical Conductivity
SAR	Sodium Adsorption Ratio
MWD	Mean Weight Diameter
RDA	Redundancy Analysis
SEM	Structural Equation Modeling
SS(GOST)	State Standards
ACMGA-4	Automatic Continuous Monitoring Gas Analyzer Model-4
MES	Electronic meteorometer stationary
MPC	maximum permissible concentrations
ASEL	Approximate safe exposure level

References

1. Bekeshev Y, Semenkov I, Stepanova Y et al (2024) Data on the temporal changes in soil properties at the emergency crash site of the launch vehicle '"Soyuz-FG"' in Kazakhstan. Data Br 55:110646. https://doi.org/10.1016/j.dib.2024.110646 - DOI
2. Bolotnik TA, Smolenkov AD, Smirnov RS, Shpigun OA (2015) Determination of rocket kerosene in soil by static headspace analysis coupled with gas chromatography–mass spectrometry. Moscow Univ Chem Bull 70:168–174. https://doi.org/10.3103/S0027131415040021 - DOI

 doi:10.20944/preprints202604.1023.v1

3. Bolotnik TA, Plyushchenko IV, Smolenkov AD et al (2018) Identification of spillages of semi-volatile hydrocarbon fuels in soils by gas chromatography-mass spectrometry. J Anal Chem 73:570–575. https://doi.org/10.1134/S1061934818060035 - DOI
4. Dallas JA, Raval S, Alvarez Gaitan JP et al (2020) The environmental impact of emissions from space launches: a comprehensive review. J Clean Prod 255:120209. https://doi.org/10.1016/j.jclepro.2020.120209 - DOI
5. Epifanov IK, Kondratyev AD, Doroshina SV (2009) Environmental damage in result of ascent-phase abort of rocket carriers. Natzional'nye Interes Prioritety i Bezop 24:53–57
6. Gennadiev AN, Pikovskii YI, Zhidkin AP et al (2015) Factors and features of the hydrocarbon status of soils. Eurasian Soil Sci 48:1193–1206. https://doi.org/10.1134/S1064229315110071 - DOI
7. Gooijer C, Kozin I, Velthorst NH (1997) Shpol'skii spectrometry, a distinct method in environmental analysis. Mikrochim Acta 127:149–182. https://doi.org/10.1007/BF01242719 - DOI
8. Hu C, Zhang Y, Zhou Y et al (2022) Unsymmetrical dimethylhydrazine and related compounds in the environment: recent updates on pretreatment, analysis, and removal techniques. J Hazard Mater 432:128708. https://doi.org/10.1016/j.jhazmat.2022.128708 - DOI
9. Ivanova E, Osipova M, Vasilieva T et al (2023) The recycling of substandard rocket fuel n, n-dimethylhydrazine via the involvement of its hydrazones derived from glyoxal, acrolein, metacrolein, crotonaldehyde, and formaldehyde in organic synthesis. Int J Mol Sci 24:17196. https://doi.org/10.3390/ijms242417196 - DOI
10. Kadono A, Funakawa S, Kosaki T (2008) Factors controlling mineralization of soil organic matter in the Eurasian steppe. Soil Biol Biochem. https://doi.org/10.1016/j.soilbio.2007.11.015 - DOI
11. Karnaeva AE, Milyushkin AL, Khesina ZB, Buryak AK (2022) 1-Methyl-1H-1,2,4-triazole as the main marker of 1,1-dimethylhydrazine exposure in plants. Environ Sci Pollut Res 29:64225–64231. https://doi.org/10.1007/s11356-022-22157-y - DOI
12. Kopack RA (2019) Rocket wastelands in Kazakhstan: scientific authoritarianism and the Baikonur cosmodrome. Ann Am Assoc Geogr 109:556–567. https://doi.org/10.1080/24694452.2018.1507817 - DOI
13. Kopack R (2021) Baikonur 2.0: 'inland-offshore' space economies in post-Soviet Kazakhstan. Cult Theory Crit 62:96–112. https://doi.org/10.1080/14735784.2021.1929363 - DOI
14. Koroleva TV, Semenkov IN, Sharapova AV et al (2021) Ecological consequences of space rocket accidents in Kazakhstan between 1999 and 2018. Environ Pollut 268:115711. https://doi.org/10.1016/j.envpol.2020.115711 - DOI
15. Koroleva TV, Semenkov IN, Lednev SA, Soldatova OS (2023) Unsymmetrical dimethylhydrazine (UDMH) and its transformation products in soils: a review of the sources, detection, behavior, toxicity, and remediation of polluted territories. Eurasian Soil Sci 56:210–225. https://doi.org/10.1134/S1064229322602001 - DOI
16. Koroleva TV, Semenkov IN, Lednev SA, Soldatova OS (2024) Jet fuel as a source of soil pollution: a review. Eurasian Soil Sci 57:1519–1524. https://doi.org/10.1134/S1064229324601264 - DOI
17. Kosyakov DS, Ul'yanovskii NV, Pikovskoi II et al (2019) Effects of oxidant and catalyst on the transformation products of rocket fuel 1,1-dimethylhydrazine in water and soil. Chemosphere 228:335–344. https://doi.org/10.1016/j.chemosphere.2019.04.141 - DOI
18. Li W, Li J, Wu Y et al (2024) Soil organic matter and bulk density: driving factors in the vegetation-mediated restoration of coastal saline lands in North China. Agron 14(9):2007. https://doi.org/10.3390/agronomy14092007
19. Liu L, Jia P, Huang Y et al (2022) Space industrialization. Environ Chem Lett 21:5571. https://doi.org/10.1007/s10311-022-01411-2 - DOI
20. Meira M, Quintella CM, Tanajura ADS et al (2011) Determination of the oxidation stability of biodiesel and oils by spectrofluorimetry and multivariate calibration. Talanta 85:430–434. https://doi.org/10.1016/j.talanta.2011.04.002 - DOI
21. Milyushkin AL, Karnaeva AE (2023) Unsymmetrical dimethylhydrazine transformation products: a review. Sci Total Environ 891:164367. https://doi.org/10.1016/j.scitotenv.2023.164367 - DOI

 doi:10.20944/preprints202604.1023.v1

22. Nguyen HN, Chenoweth JA, Bebarta VS et al (2021) The toxicity, pathophysiology, and treatment of acute hydrazine propellant exposure: a systematic review. Mil Med 186:e319–e326. https://doi.org/10.1093/milmed/usaa429 - DOI
23. Pikovskii YI, Korotkov LA, Smirnova MA, Kovach RG (2017) Laboratory analytical methods for the determination of the hydrocarbon status of soils (a review). Eurasian Soil Sci 50:1125–1137. https://doi.org/10.1134/S1064229317100076 - DOI
24. Federal Aviation Administration (FAA). Final Environmental Assessment and Finding of No Significant Impact (FONSI) for the SpaceX Falcon Program (LC-39A & LC-40, Kennedy Space Center / Cape Canaveral). Washington, DC: FAA Office of Commercial Space Transportation, **2020**, ~600 pp.
25. Federal Aviation Administration (FAA). Draft Environmental Assessment: SpaceX Falcon 9 Operations at Space Launch Complex 40, Cape Canaveral Space Force Station, Florida (with Air Quality Technical Report). Washington, DC: FAA, **March 2025**, 300+ pp.
26. National Aeronautics and Space Administration (NASA); U.S. Air Force (USAF). *Environmental Assessment — SpaceX Falcon 1 and 9 Launch Programs at CCAFS/KSC.* Washington, DC: NASA/USAF, **2007**, 300+ pp. (Supplemental EA, 2013; FONSI for F9 RTLS, 2015.)
27. CNES / Centre Spatial Guyanais (CSG). *Environmental Measurement Plan (EMP) & Annual Environmental Reports (Ariane/Vega).* Kourou, French Guiana: CNES/CSG, **2012–2023**, multi-year report series, page counts vary.
28. Chanoine, A. (for ESA Clean Space). *Environmental impacts of launchers and space missions — Life Cycle Assessment (LCA).* Clean Space Industrial Days (CSID), **2017**, 35 pp. (conference presentation/materials).
29. Xue, Y.; John, R.; et al. **(2021).** Rocket launching activities are associated with reduced insect species richness and abundance in two types of tropical plantations around the Wenchang Satellite Launch Center, southern China. Ecological Indicators, 127, Article 107751, pp. 1–10, **2021**.
30. China Aerospace Studies Institute (CASI), Air University. *China's Ground Segment.* Maxwell AFB, AL: Air University Press, **2021** (March 1), 80+ pp.
31. Philippine Space Agency (PhilSA). *Advisory on the Long March 8A rocket launch (drop-zone and maritime safety notice).* Manila: PhilSA (official advisory), **2025** (August 26).